Journal of Inflammation Research

Dovepress
Taylor & Francis Group

Open Access Full Text Article

ORIGINAL RESEARCH

Role of Monocyte/Macrophage-Associated Gene Ccl9 in Acute Myocardial Infarction Analysis: Based on Bulk and Single Cell RNA Sequencing Data

Qiang Yang[1], Ziyue Luo[2], Xinyi Cheng[2], Tianyu Wang[2], Pengfei Hu[1]

[1]Department of Cardiology, The Second Affiliated Hospital of Zhejiang Chinese Medical University, Hangzhou, Zhejiang, 310005, People's Republic of China; [2]Second Clinical Medical College, Zhejiang Chinese Medical University, Hangzhou, Zhejiang, 310053, People's Republic of China

Correspondence: Pengfei Hu, Department of Cardiology, The Second Affiliated Hospital of Zhejiang Chinese Medical University, Hangzhou, Zhejiang, 310005, People's Republic of China, Tel +86 15267037741, Email 20064012@zcmu.edu.cn

Background: Acute myocardial infarction (AMI) is one of the major causes of sudden cardiac death, resulting in severe complications. Therefore, it is of great significance to find new therapeutic targets.

Methods: AMI datasets, Bulk RNA sequencing (Bulk RNA seq) GSE158157 and GSE23294, scRNA-seq GSE163129 datasets were downloaded from GEO. In this study, GSE163129 was subjected to dimensionality reduction analysis, subpopulation identification, enrichment analysis, and cellular communication analysis. Subsequently, we performed differential expression and immune infiltration analysis on GSE158157 and GSE23294 datasets to obtain seven monocyte/macrophage-related core genes. Finally, the mechanism of Ccl9 in AMI was explored through a series of animal and cellular experiments, which involved the establishment of AMI mouse model and isolation of primary mouse cardiomyocytes.

Results: The t-distributed stochastic neighbor embedding (tSNE) analysis of GSE163129 identified 18 cell clusters, divided into six cell types. Monocytes and neutrophils were highly active. Differential expression analysis of GSE158157 and GSE23294 identified 2362 differentially expressed genes (DEGs). Immune infiltration analysis showed macrophage presence, with notable differences in M2 monocytes and other immune cells between AMI and Sham groups. Nine monocyte-associated hub genes were identified. qRT-PCR validation in AMI mouse models revealed significant upregulation of B2M, SPP1, Ccl4, LGALS3, MRC1, Ccl9, and FN1. Co-culture of primary cardiomyocytes and RAW264.7 cells indicated that low Ccl9 expression promoted M2 macrophage polarization and reduced OGD-induced cardiomyocyte injury.

Conclusion: This study identified seven monocyte/macrophage-related genes in AMI and highlighted Ccl9's potential role in regulating M2 macrophage polarization and mitigating OGD-induced cardiomyocyte injury in AMI.

Keywords: acute myocardial infarction, Ccl9, monocyte, macrophage, ScRNA-seq

Introduction

Cardiovascular diseases have emerged as the leading cause of death worldwide, accounting for 45% of all mortalities.[1] Acute Myocardial Infarction (AMI) is a critical cardiovascular condition that poses a significant threat to human life and is one of the leading causes of sudden cardiac death. Additionally, the poor prognosis of AMI is most likely due to partially understood pathophysiological mechanisms.[2]

The ongoing advancement of interventional techniques has greatly enhanced the diagnosis and treatment of AMI, however the progress of the pharmacological treatment of AMI remains slow. Therefore, there is an urgent need to explore the important mechanisms of action and key genes in the development of AMI, in order to excavate possible pharmacological treatments for AMI. Recently studies have shown that inflammation plays a major role in the pathophysiological mechanisms of AMI.[3] It has been found that a pro-inflammatory response occurs early in AMI,

Received: 15 January 2025
Accepted: 26 September 2025
Published: 31 October 2025

which aims to remove necrotic cell debris from the infarcted area of the myocardium.[4] The pro-inflammatory response is followed by an anti-inflammatory and pro-repair phase, which promotes wound healing and scar formation, thereby preventing cardiac rupture.[4] The transition between these two phases is accomplished by relying on the complex regulation of multiple cells and inflammatory cells within the heart. Monocytes/macrophages are among the most important cells involved in the regulatory process.[5] During the initial phase of AMI, monocytes present in the bloodstream are subjected to various inflammatory chemokines, as a result, they rapidly migrate to the site of myocardial infarction and differentiate into macrophages, actively contributing to the inflammatory response.[6] As time progresses, macrophages are further polarized to produce M1 macrophages, which play a major role in the pro-inflammatory phase, and M2 macrophages, which play a major role in the anti-inflammatory and pro-repair Phase[6] Therefore, it is evident that monocytes/macrophages are greatly involved in the two important phases of the inflammatory response and that the balance between the pro-inflammatory and anti-inflammatory and pro-repair phases is of great significance for a range of pathophysiological processes after AMI.

Bioinformatics plays a major role in the study of pathophysiological related processes in various diseases. A study found that AMI is accompanied by dysregulation of multiple biological functions through Bulk RNA sequencing (Bulk RNA seq) and bioinformatics analysis.[7] Furthermore, there have been studies are exploring endothelial cells with specific immune characteristics during AMI and their potential role in adverse cardiac remodeling through Single cell RNA sequencing (scRNA-seq) data.[8] Nevertheless, Bulk RNA seq and scRNA-seq have their own advantages and disadvantages, where Bulk RNA seq is able to assess the average gene expression information of the overall cell population but is unable to differentiate between individual cells. In contrast, scRNA-seq offers detailed high-resolution single-cell information and can resolve cellular heterogeneity but lacks the characterization of the overall cell population. Therefore, combining the strengths and complementing the weaknesses of both may be a more desirable analysis method.

Therefore, it is of great significance to explore the pathophysiological mechanisms associated with AMI inflammation to find new therapeutic targets. In this study, we found the key genes of monocytes/macrophages in AMI by single cell binding to the Bulk transcriptome, which was validated by animal and cellular experiments, and elucidated the potential interactions between macrophages and cardiomyocytes, which enriched the study of pathophysiological mechanisms related to AMI inflammation.

Methods

Acquisition and Processing of Datasets

The mouse AMI single-cell transcriptome sequencing dataset GSE163129 was downloaded from the GEO database (https://www.ncbi.nlm.nih.gov/geo/), and the source of tissue samples was myocardial immune cells. Single-cell analyses were performed using the Seurat package (V4.3). Mouse AMI Bulk datasets GSE158157 and GSE23294 were downloaded (Containing partial microarray data), where the sample source was myocardium. Data were normalized using limma (V3.56) in R (V4.3.0) and batch effects were removed from the datasets using SVA (V 3.48).

Dimensionality Reduction Analysis and Subpopulation Identification of Single-Cell Datasets

Cells exhibiting gene expression values below 200 and above 6000 were excluded, and cells annotated as endothelial cells were excluded based on the original reference.[9] The t-distributed stochastic neighbor embedding (tSNE) analysis was selected, with the clustering RESOLUTION set to 0.5 and 18 cell clusters in the co-cluster. The cell clusters were annotated using the ImmGenData database in celldex (V 1.10). Differentially Expressed Genes (DEGs) analysis was performed using FindAllMarkers to find DEGs in each cell cluster, and the Top 10 DEGs of each cell cluster were selected to draw heatmaps.

Screening of DEGs in Single Cell Data

Difference analysis was performed to compare AMI and Sham. DEG analysis was performed for genes in each cell type using a threshold set at |log2FC|>1and adj. pvalue<0.05.

Functional Enrichment Analysis

Gene Ontology (GO) and Kyoto Encyclopedia of Genes and Genomes (KEGG) enrichment analyses were performed on DEGs using the clusterProfiler package and the org.Mm.eg.db package, with pvalue and adjust pvalue < 0.05 set.

Intercellular Communication Analysis

Correlation analysis of cellular communication was performed using CellChat (V 1.6.1).

Screening of Bulk Dataset DEGs

DEG analysis of samples was performed using the limma package of R (V 4.3.0), with thresholds set to |log2FC|>1 and adjust pvalue<0.05. Volcano mapping was performed using the ggplot package (V 3.4), whereas heatmapping was performed using the pheatmap package.

Immuno-Infiltration Analysis

Immune infiltration analysis was performed using the CIBERSORT package, thereafter the differences in expression of 22 immune cells in AMI vs Sham were plotted.

Screening and Analysis of Hub Genes

The DEGs in Monocytes cell types in single cells were intersected with those of bulk to further obtain Monocytes-related DEGs. Protein-Protein Interaction Networks (PPI) were constructed for DEGs using the STRING database, thereafter the number of nodes of the network was plotted and the Top 15 nodes selected. Receiver operator characteristic (ROC) curves were plotted using the multipleROC calculation and plot_ROC in multiple ROC (V 0.1). Genes with Area Under Curve (AUC) values greater than 0.75 and pvalue < 0.05 were selected and defined as Monocytes-associated hub genes. Correlations between hub genes and monocytes in bulk data were calculated using corr.test in the psych package (V2.3), and correlation analyses were performed using spearman analysis. Single gene Gene Set Enrichment Analysis (GSEA) enrichment analysis of hub genes was performed using gseKEGG in clusterProfiler (V4.8).

Establishment of AMI Model

The animal experiments in this study were approved by the Animal Care and Use Committee of Hangzhou Medical College (No. ZJCLA-IACUC-20010502) and conformed to the "Guide for the Care and Use of Laboratory Animals". Male C57BL/6 mice weighing 15–25 g were selected and randomly divided into two groups: Sham and AMI groups. The mice in the AMI group were subjected to ligation of the left anterior descending branch (LAD) to simulate AMI. The procedure involved administering anaesthesia using ketamine hydrochloride (100 mg/kg/bw) and xylazine (10 mg/kg/bw). Following the sufficient administration of anaesthesia, mice were intubated and connected to a small animal ventilator. After dehairing, the chest area was cleaned using povidone-iodine and isopropyl alcohol prewash. After open-chest surgery, the LAD was ligated using 8–0 silk thread to simulate AMI then open-chest incision was closed after surgery. The Sham group was operated similarly to the AMI group but without ligation of the LAD.[10] The model was evaluated 24 hours after its creation using relevant tests applicable for assessing its performance. These tests included analysis of both heart and peripheral blood serum samples. Carbon dioxide was used for execution. Other tests were performed 72h after modelling.

2,3,5-Triphenyltetrazolium Chloride (TTC) Staining

The hearts of different groups of mice were frozen in a −80°C refrigerator for 8 min, and then cut into five round slices of 0.1–0.3 cm thick. Subsequently, the slices were immersed in TTC solution (Sigma Aldrich, USA) and incubated for 30 min at 37°C. The slices were protected from light, and then fixed in 4% formaldehyde for 24 h. Finally, the slices were arranged in order from largest to smallest, and the size of myocardial infarction area was observed.[11]

Hematoxylin and Eosin (H&E) Staining

Heart tissues were fixed in a 10% formaldehyde (Sigma Aldrich, USA) and then embedded in paraffin. Sections were then cut into 5 μm sections using a microtome. After dewaxing and dehydration, the sections were stained with Hematoxylin and eosin. The sections were then observed using a microscope (Olympus, Japan).

Determination of Myocardial Injury Markers and Inflammatory Factors

Serum or cell culture supernatant samples were collected. CK (abbexa, UK), CKMB (abx153828, abbexa, UK), cTnI (abx154780, abbexa, UK), IL-6 (abbexa, UK), IL-1β (Nanjing Jiancheng, China), IL-10 (abbexa, UK), TNF-α (Nanjing Jiancheng, China) ELISA kits were used to detect myocardial injury markers and inflammatory factors.

Immunofluorescence Staining

Cardiac tissues were fixed in 10% formaldehyde and then embedded in paraffin. Tissue sections with a thickness of 2 μm thick were incubated with iNOS (1:100, Abcam, UK), CD206 (1:100, Abcam, UK), CD68 (1:100, Abcam, UK), and then incubated with DAPI (1 μm/mL) (Sigma Aldrich, USA) for 15 min in the dark. Finally, images were observed in a dark room and captured using fluorescence microscopy (Olympus, Japan) with a magnification of 200 x. The tissues were then incubated with DAPI (1 μm/mL) for 15 minutes in the dark.

Quantitative Real-Time Polymerase Chain Reaction (qRT-PCR)

Total RNA from myocardial tissue was extracted using Trizol reagent (Thermo Fisher, USA), which was subsequently reverse transcribed to cDNA (Takara, China). qRT-PCR was performed using qPCR (Takara, China). gAPDH was used as an internal control for mRNA. Gene expression was calculated using the 2-ΔΔCT method. Primer sequences are detailed in the Supplementary Material (Supplementary Table 1).

Isolation and Culture of Primary Cardiomyocytes

Primary mouse cardiomyocytes were isolated from C57BL/6 mice aged 1–3-day. The ventricles were dissected and minced into pieces with an area of 1 mm^3 and digested using 0.2% collagenase II on ice for 2 hours. The digested tissue was pipetted and filtered through a 70 μm filter. Cells were collected and cultured in DMEM (Gibco, USA) containing 10% fetal bovine serum (Corning, USA).[12]

Cell Transfection

RAW264.7 cells were provided by Shanghai Saiding Biotechnology. The cells were inoculated into culture flasks at 3×10^5/mL and cultured in DMEM containing 10% FBS (Corning, USA) at 37°C in a 5% CO2 incubator (Gibco, USA). Cell passaging was performed at 70–80% confluence. Lentiviruses containing Ccl9 shRNA (shRNA-Ccl9) as well as negative control shRNA (shRNA) were obtained from Obio Technology (Shanghai). Ccl9 knockdown was performed by transfection of shRNA-Ccl9 lentiviruses in RAW264.7 cells. Transfection efficiency was measured using qRT-PCR (Supplementary Figure 1).

Induction of M2 Macrophages

RAW264.7 cells exposed to IL-4 (20 ng/mL) were stimulated for 24h for M2 differentiation.[13] The groupings were: RAW264.7, RAW264.7+shRNA, RAW264.7+IL-4, RAW264.7+IL-4+shRNA and RAW264.7+IL-4+shRNA-Ccl9.

Establishment of Oxygen-Glucose Deprivation (OGD) Model

Primary mouse cardiomyocytes were cultured in glucose-free DMEM containing 1% O_2 at 37°C to construct the OGD model.

RAW264.7-Mouse Primary Cardiomyocyte Co-Culture[14]

Primary cardiomyocytes and RAW264.7 cells were co-cultured, and the medium after M2 macrophage induction was discarded. The cells were washed twice with phosphate-buffered saline (PBS), then fresh medium was added. The culture was maintained for 24 h. Conditioned medium was collected for RAW264.7 (CM0), RAW264.7+shRNA (CM1), RAW264.7+IL-4 (CM2) and RAW264.7+IL-4+shRNA (CM3). The conditioned medium was filtered with a filter (Millipore, Billerica, MA, USA), and then added to OGD-modelled primary cardiomyocytes and incubated for 24 h. Groupings were: control (OGD+CM0), OGD+CM1, OGD+CM2 and OGD+CM3.

Cell Counting Kit-8 (CCK-8) Assay

Cell viability was measured using CCK-8 (96992, Sigma Aldrich, USA). The groups of cells were inoculated in 96-well plates at a density of 1×10^5 cells/well. After treatment, CCK-8 reagent was added and absorbance at 450 nm was assessed using an enzyme marker (Bio-Rad, Hercules, CA).

Calculation of Primary Cardiomyocytes for Apoptosis Levels

Apoptosis was measured using the Annexin V-FITC/PI Apoptosis Detection Kit (559763, BD Bioscience, USA). Primary cardiomyocytes were harvested and washed with PBS and then resuspended in 500 μL of binding buffer at a concentration of 1×106/mL. Cells were then incubated with membrane-bound protein V-FITC and PI for 15 min. Data were analysed using a FACSCalibur flow cytometer (BD Biosciences, USA).

Statistical Analysis

Analyses were performed using GraphPad Prism (V8.02). The Shapiro–Wilk normality test to determine data distribution. Unpaired *t*-tests were used to compare differences between groups. pvalue<0.05 represents statistical significance.

Results

Subcluster Identification of Single-Cell Datasets

In this study, 18 cell clusters were co-classified by tSNE analysis and annotated into 6 cells types: Macrophages, Neutrophils, Monocytes, B cells, T cells, NK cells (Figure 1A–D). Heatmaps were generated by selecting the Top 10 DEGs of each cell cluster (Figure 1E).

Screening and Enrichment Analysis of Cell Cluster DEGs

We counted the proportion of different cell types in the two groups (Figure 2A) and screened the DEGs of each cell type, and finally obtained a total of 1002 DEGs. A total of 199 DEGs were found in Macrophages, 339 DEGs in Neutrophils, 283 DEGs in Monocytes, 43 DEGs in B cells, 81 DEGs in T cells and 58 DEGs in NK cells (Figure 2B). The GO enrichment showed that the DEGs mentioned above were mainly enriched in regulation of macrophage migration, regulation of granulocyte chemotaxis, and monocyte differentiation (Figure 2C). KEGG enrichment analysis revealed that the above DEGs were mainly enriched in Th17 cell differentiation, Th1 and Th2 cell differentiation and T cell receptor signaling pathway (Figure 2D).

Analysis of Intercellular Communication

To investigate the interactions between the six cell types, the number of communications and the intensity of communications between them were analyzed separately (Figure 3A and B). The results showed that Monocytes and Neutrophils had the highest number of cellular communications (Figure 3C). Additionally, this study found that Ccl9 signaling pathway plays a crucial role in cell communication (Figure 3D).

Screening and Enrichment Analysis of DEGs in Bulk Dataset

The Bulk dataset was combined using normalization and de-batching techniques (Figure 4A–D), resulting in the identification of 2362 DEGs were screened using intergroup DEG analysis. Among these DEGs, 2246 were up-

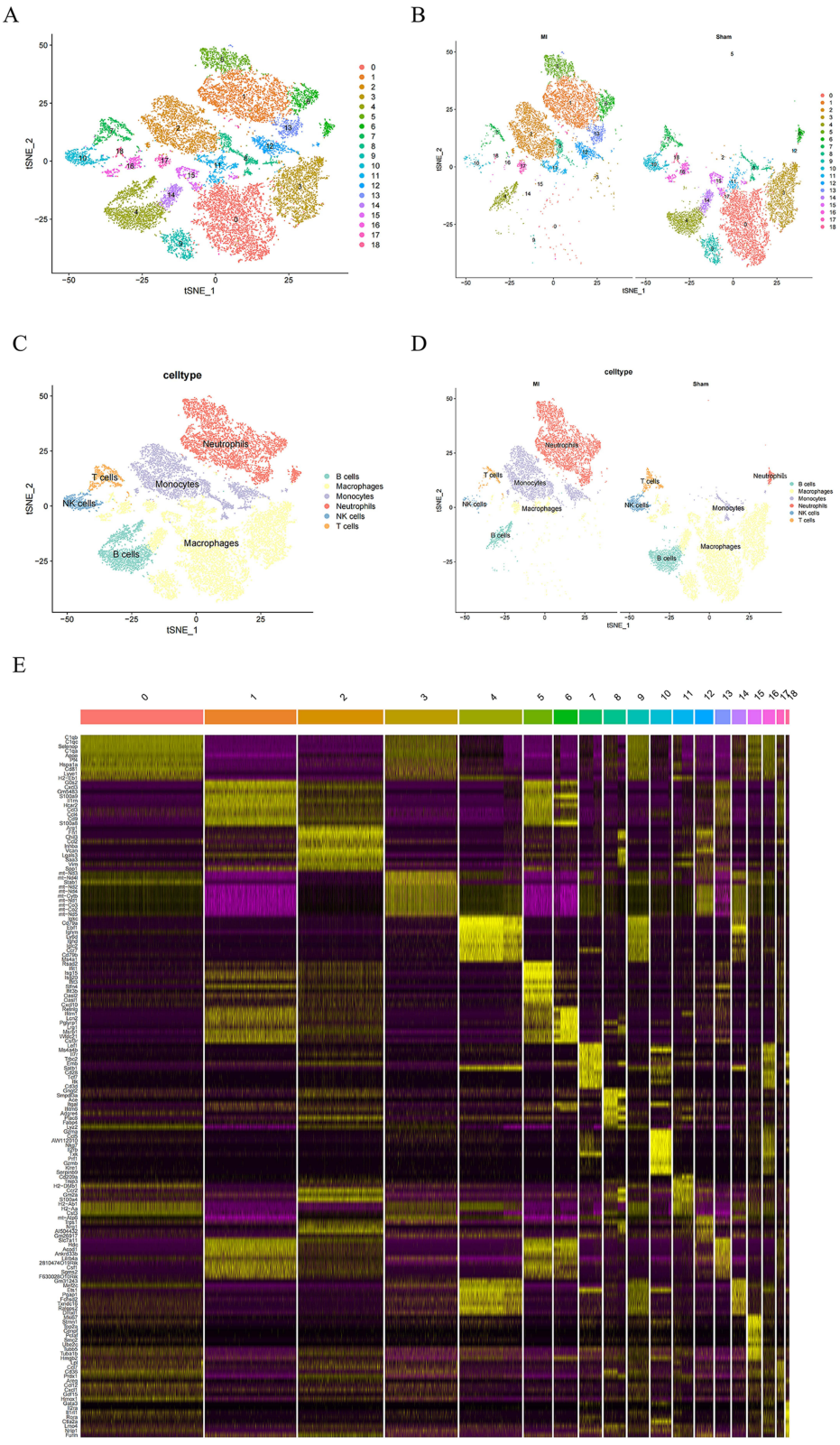

Figure 1 Subcluster identification as well as visualisation of the single cell dataset. (**A** and **B**) A total of 18 cell clusters were classified using tSNE analysis; (**C** and **D**) A total of 6 cell types were annotated using celldex, namely Macrophages, Neutrophils, Monocytes, B cells, T cells, and NK cells; (**E**) Heatmaps drawn by Top 10 DEGs for each cell cluster.

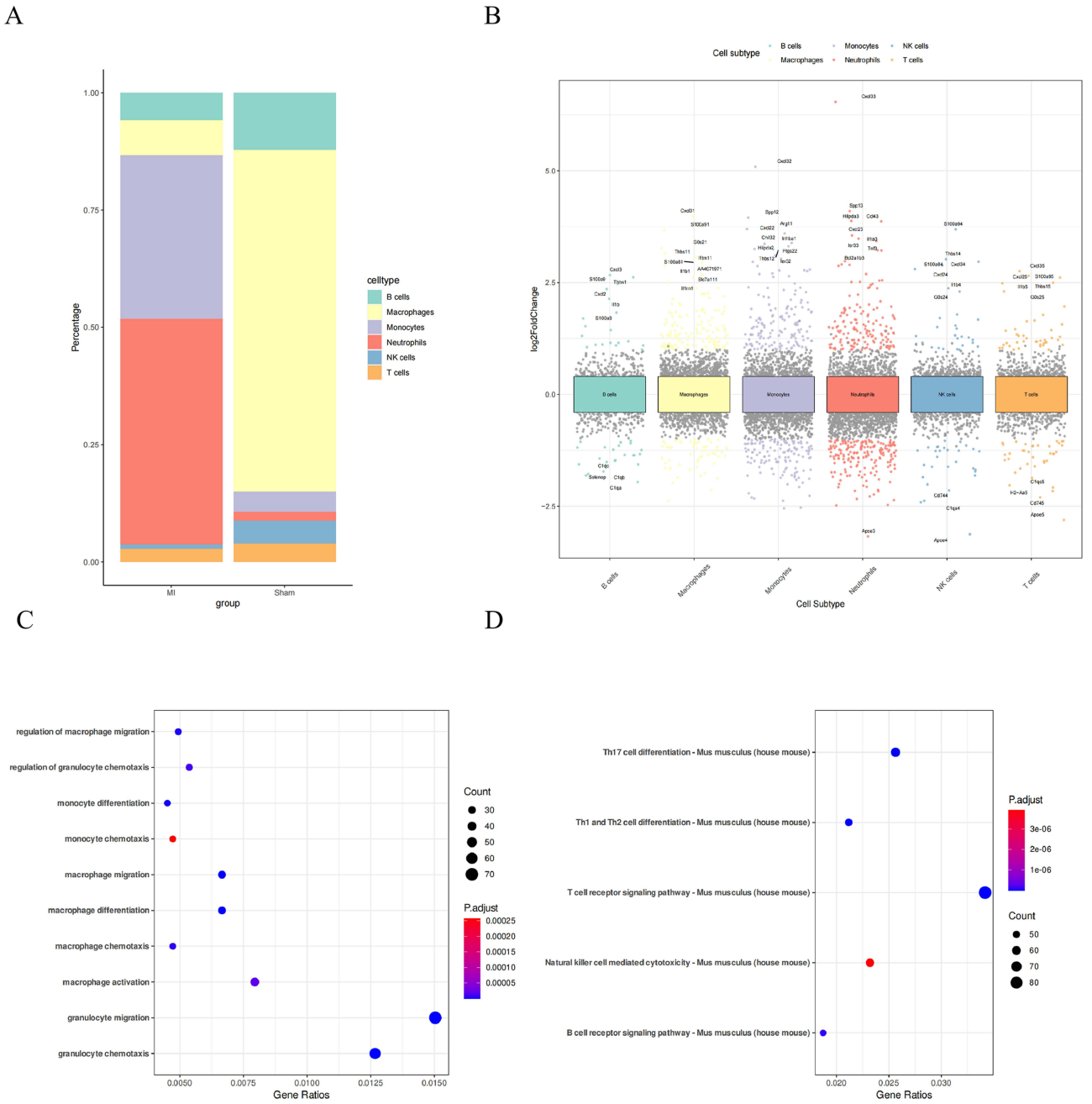

Figure 2 Screening as well as enrichment analysis of DEGs of cell clusters in the single-cell dataset. (**A**) Histogram of the percentage of cell species between AMI VS Sham groups; (**B**) DEGs of 6 cell types between AMI VS Sham groups; (**C**) Bubble plot of GO enrichment analysis of AMI VS Sham DEGs; (**D**) Bubble plot of KEGG enrichment analysis of AMI VS Sham DEGs.

regulated genes and 116 were down-regulated genes (Figure 4E and F). The enrichment results showed that GO analysis mainly enriched in generation of precursor, metabolites and energy, ribose phosphate metabolic, mitochondrial, protein-containing complex, actin binding. Additionally, KEGG analysis predominantly revealed enrichment in pathways of neurodegeneration (Figure 4G and H).

Analysis of Immune Infiltration

Differential analysis of 22 immune cells in this study revealed that Eosinophils, active Mastoells, resting Mastoells and macrophages. M2, monocytes, gamma delta T cells. The levels of CD4 memory resting cells showed substantial differences

https://doi.org/10.2147/JIR.S516092

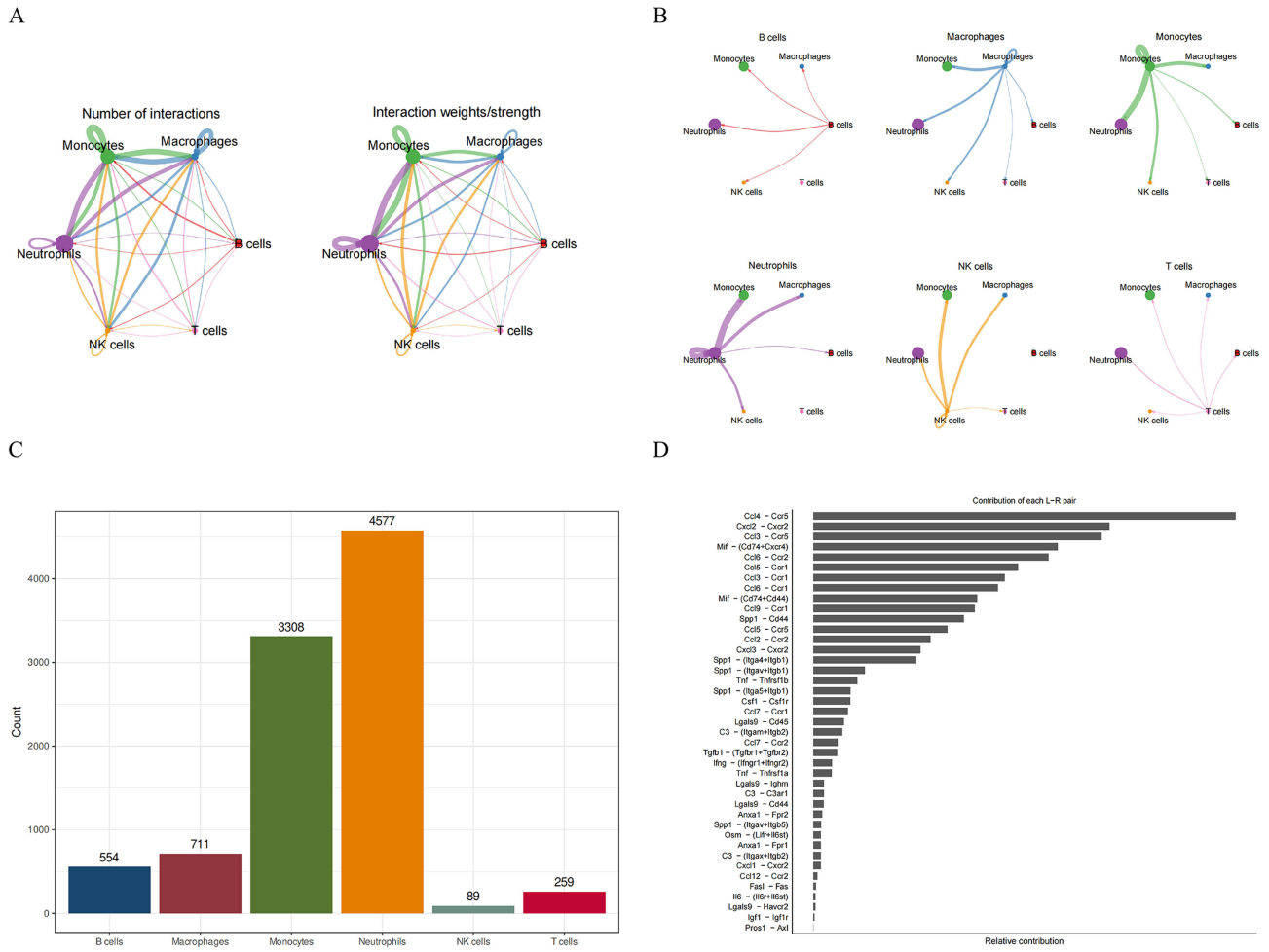

Figure 3 Analysis of cellular communication between each cell species. (**A** and **B**) Cell communication analysis of six cell types using CellChat; (**C**) Histogram of the number of cell communication among six cell types; (**D**) Role of each ligand-receptor (L-R) pair in the cell-cell communication network.

across groups (Figure 5A and B). Subsequently, this study analyzed the correlation of immune cells in AMI (Figure 5C). Primary screening was done on Monocytes-related hub genes. In this study, we took the intersection of DEGs in bulk dataset and DEGs of Sham vs AMI in Monocytes in single-cell dataset. A total of 97 Monocytes-associated DEGs were identifies (Figure 6A). Subsequently, this study performed PPI analysis on 97 Monocytes-related DEGs to select core nodes, and selected Top 15 DEGs, which were Ccl2, Cxcl1, Cd14, Gapdh, Ccr5, Arg1, Lgals3, Mrc1, Fcgr3, Ccl4, Fn1, Spp1, Apoe. Ccl9, B2m (Figure 6B). Subsequently, AUC analysis was performed on 15 nodes to screen Monocytes-related hub genes based on AUC values > 0.75 with pvalue < 0.05, which were Gapdh, Lgals3, Mrc1, Fcgr3, Ccl4, Fn1, Spp1, Apoe, Ccl9, B2m (Figure 7).

Validation of Monocytes-Associated Hub Genes and Single-Gene GSEA

This study aimed to validate the original dataset of Monocytes-associated hub genes. It was shown that the expression of all the above hub genes was found to be statistically significant (Figure 8A). Consequently, our study excluded Gapdh by Monocytes correlation analysis (Figure 8B). Single-gene GSEA showed that Monocytes-associated hubs mainly play a role in inflammatory and immune-related functions and pathways, such as Neutrophil extracellular trap formation, TNF signaling pathway, and IL-17 signaling pathway (Supplementary Figure 2).

Establishment and Evaluation of AMI Mouse Model

The present study involvement of a mouse model of AMI through ligation of the LAD followed by the assessment of the modelling process. Mice in the AMI group showed significantly higher levels of myocardial injury markers CKMB,

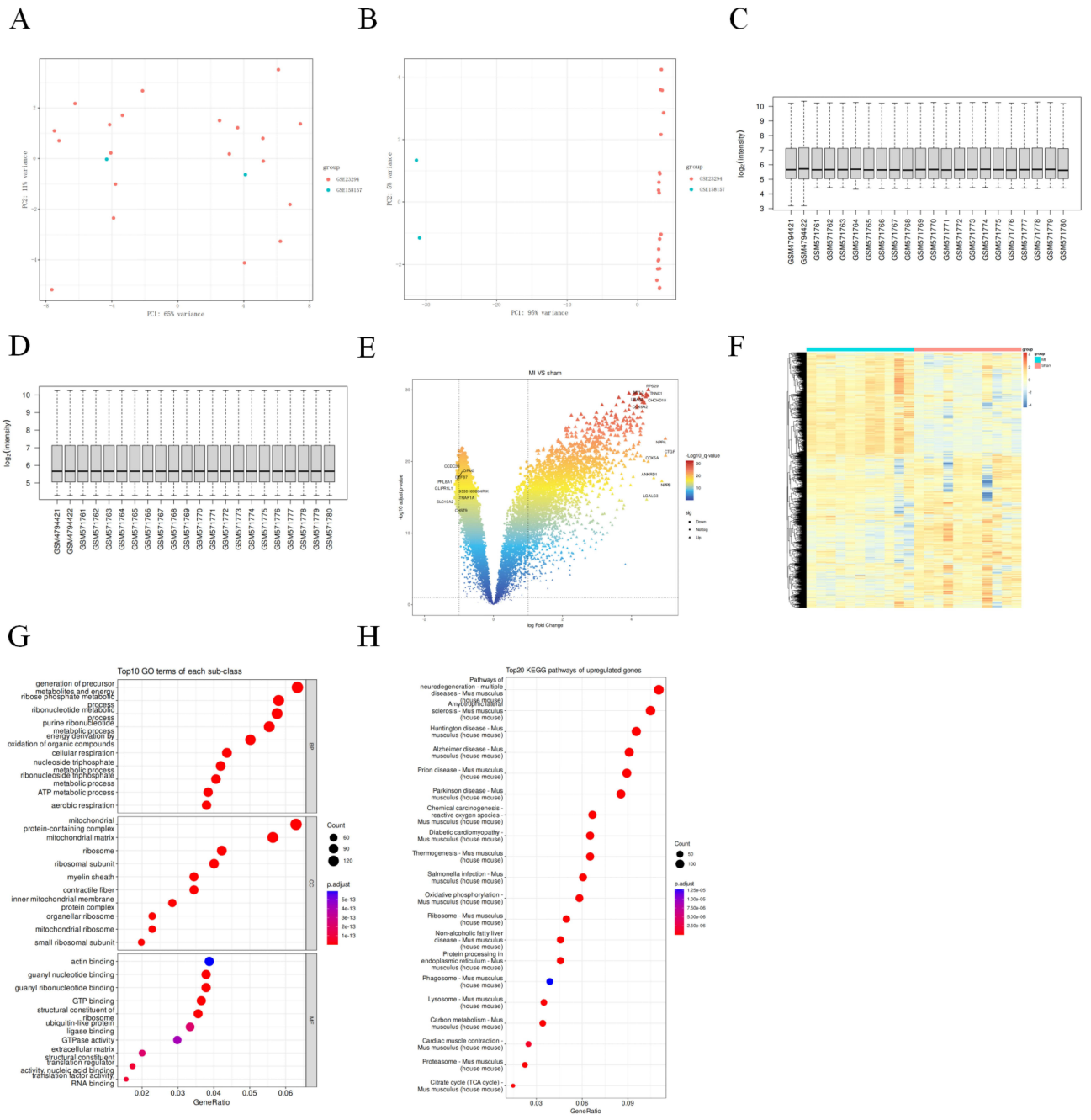

Figure 4 Screening and enrichment analysis of DEGs for Bulk dataset. (**A** and **B**) Data normalisation on Bulk dataset; (**C** and **D**) Data de-batching on Bulk dataset; (**E**) Volcano plots of DEGs between AMI VS Sham groups (|log2FC| > 1 and adjusted p-value < 0.05); (**F**) Heatmaps of DEGs between AMI VS Sham groups; (**G**) Bubble plots of GO enrichment analysis of DEGs between AMI VS Sham groups; (**H**) Bubble plots of KEGG enrichment analysis of DEGs between AMI VS KEGG enrichment analysis bubble plots for DEGs between Sham groups.

CTnI, and CK compared with the Sham group ($P < 0.01$) (Figure 9A–C), as well as significantly higher levels of inflammatory markers IL-6, IL-1β and TNF-α ($P < 0.001$) (Figure 9D–F). The TTC staining revealed partial whitening of the heart and the existence of infarcts in the AMI group, while no infarcts were observed in the Sham group (Figure 9G) (Supplementary Figure 3). HE staining showed that myocardial fibre breaks and infiltration of inflammatory cells were present in the AMI group, whereas no obvious abnormality was seen in the Sham group (Figure 9H). Immunofluorescence assay showed the presence of M1 macrophages (CD68, iNOS) and M2 macrophages (CD68, CD206) infiltration in myocardial tissues of mice in the AMI group (Figure 9I).

https://doi.org/10.2147/JIR.S516092

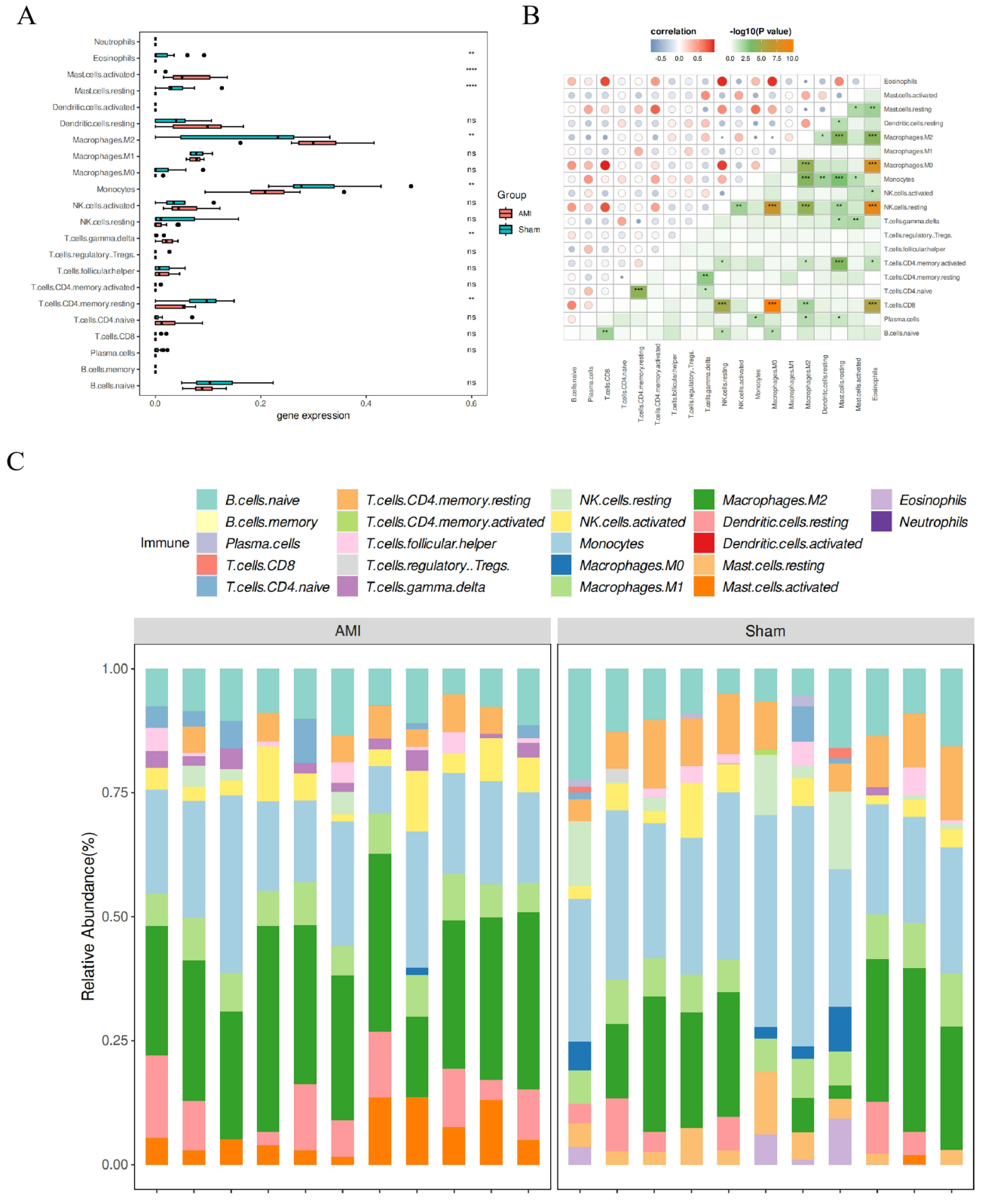

Figure 5 Immune infiltration analysis of the Bulk dataset. (**A**) Box plot of the expression of 22 immune cells in AMI VS Sham; (**B**) Heat map of the interactions between immune cells with differential expression between AMI VS Sham groups; (**C**) Histogram of the percentage of 22 immune cells between samples in AMI VS Sham. (AMI VS Sham: *p < 0.05; **p < 0.01; ***p < 0.001; ****p < 0.0001; ns, no significance).

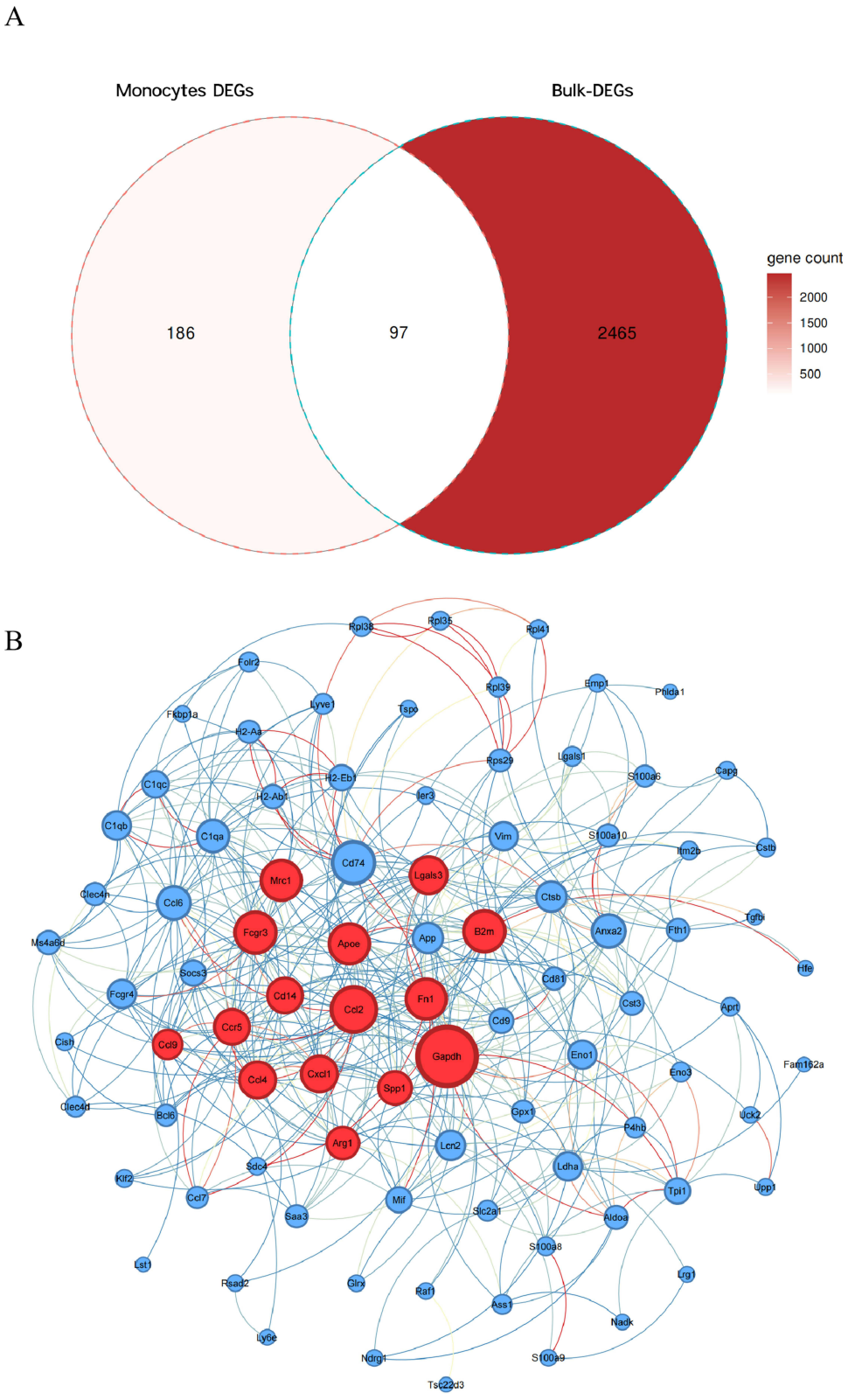

Figure 6 Initial screening of Monocytes-associated hub genes. (**A**) Wayne plots of DEGs of Monocytes cells from the single-cell dataset versus DEGs from the Bulk dataset taken as intersections; (**B**) PPI network of 97 Monocytes-associated DEGs.

https://doi.org/10.2147/JIR.S516092

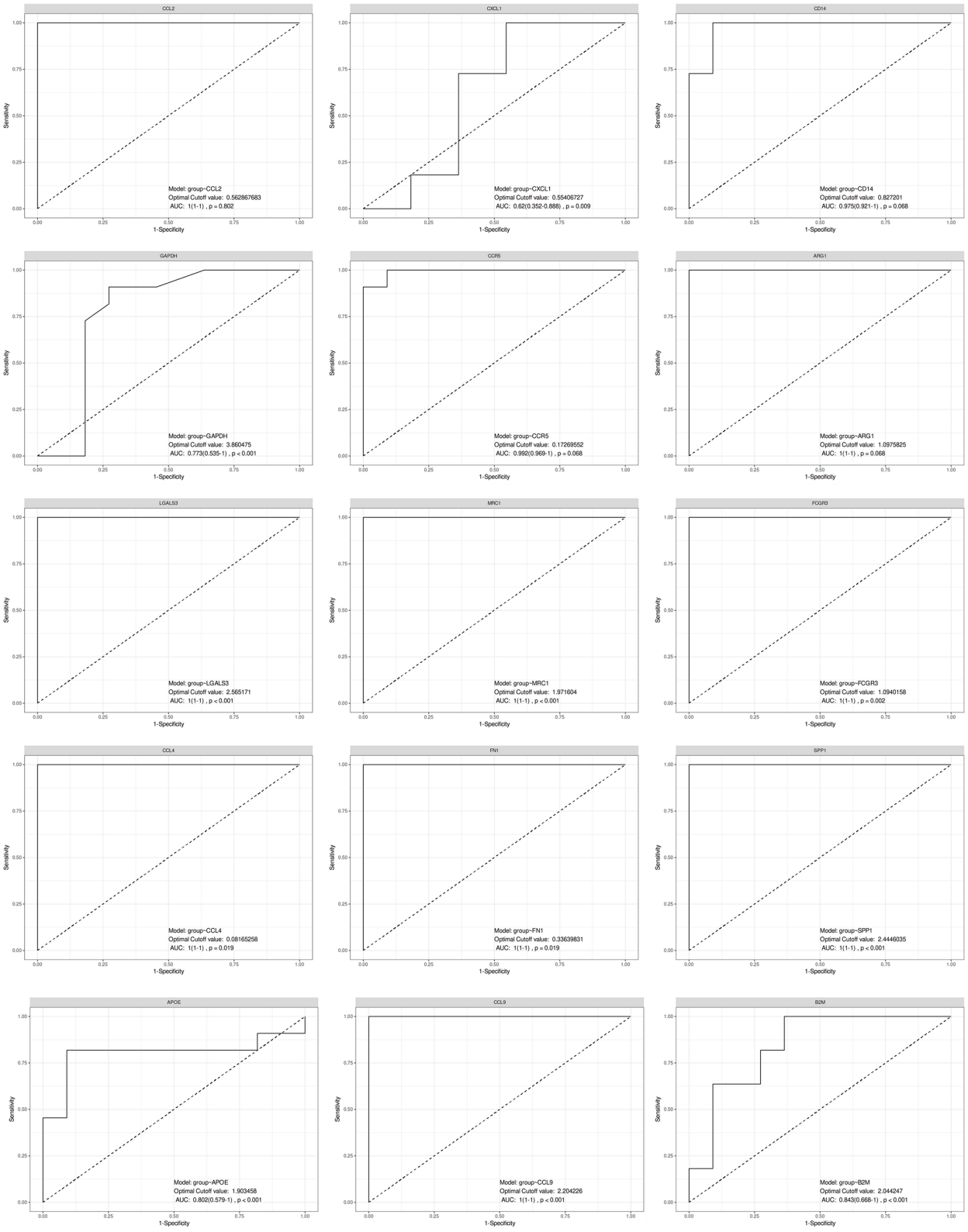

Figure 7 AUC analysis of Top 15 DEGs.

Animal Experimental Validation of Monocytes-Related Hub Genes

The study utilized qRT-PCR to validate 9 Monocytes-related hub genes. The results showed that B2M, SPP1, Ccl4, LGALS3, MRC1, Ccl9, and FN1 were significantly highly expressed in the myocardial tissues of mice with AMI, which

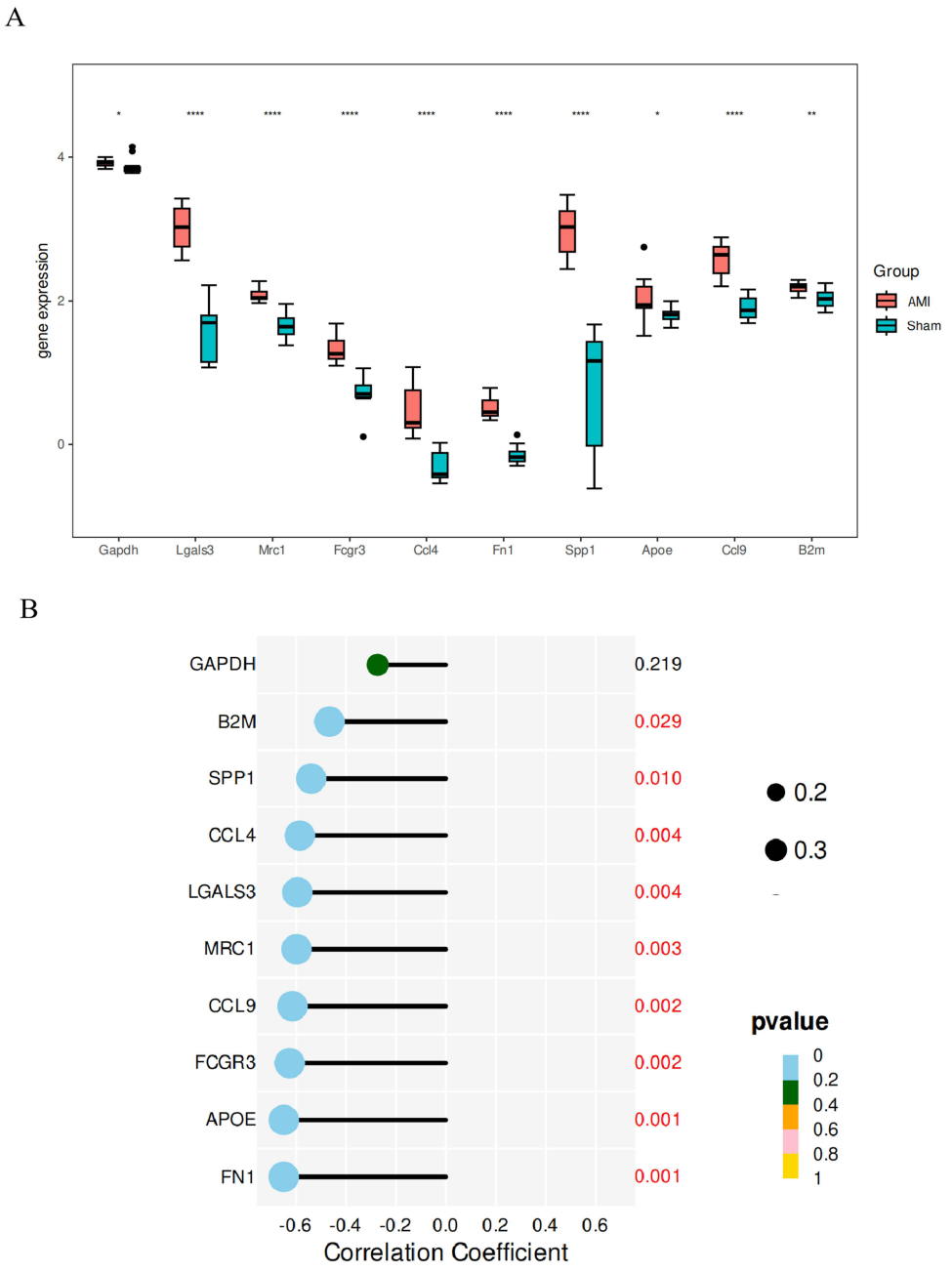

Figure 8 Validation of Monocytes-related hub genes. (**A**) Validation of the expression of Gapdh, B2m, Spp1, Ccl4, Lgals3, Mrc1, Ccl9, Fcgr3, Apoe, and Fn1 in the original dataset; (**B**) Correlation analysis between Gapdh, B2m, Spp1, Ccl4, Lgals3, Mrc1, Ccl9, Fcgr3, Apoe, and Fn1 and the Monocytes were analysed for correlation. (AMI VS Sham: *p < 0.05; **p < 0.01;;****p < 0.0001).

was consistent with the results of the BioBelief analysis (P<0.001). However, FCGR3 and APOE showed no significant differences between the AMI group and Sham group (P > 0.05) (Figure 10A–I).

Ccl9 Modulates Raw264.7 M2 Polarization Levels Thereby Affecting OGD-Induced Primary Cardiomyocyte Injury in Mice

In this present study, we manipulated expression level Ccl9 in Raw264.7 cells followed by M2 polarization induction. We observed that the anti-inflammatory factor IL-10 was significantly higher in the induced IL-4 group than in the control group where no induction was performed (P<0.001). Furthermore, IL-10 levels were significantly higher in the IL-4 +shRNA-Ccl9 group compared to the IL-4 group (P<0.05). However, there was no significant difference between IL-4

https://doi.org/10.2147/JIR.S516092

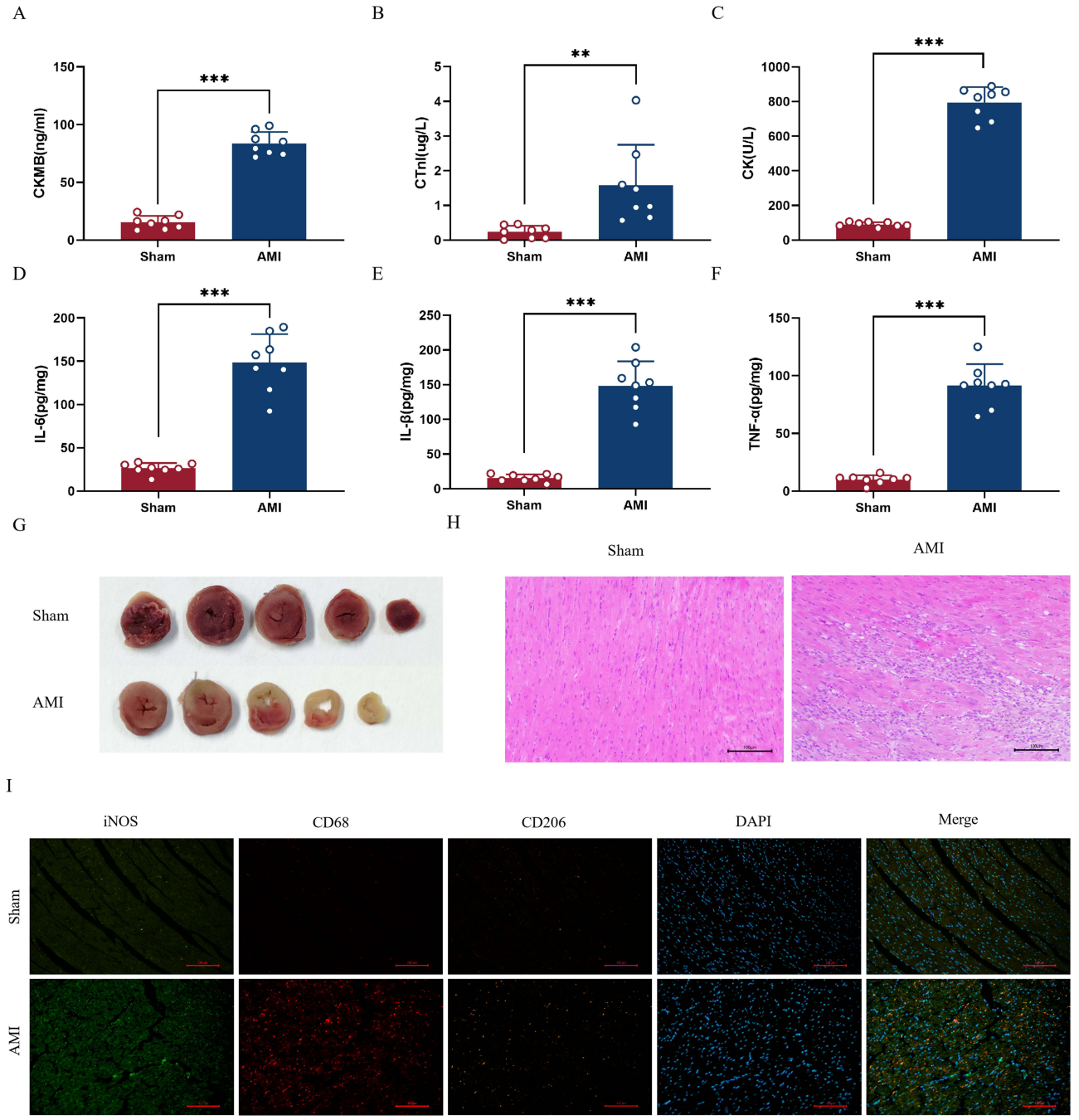

Figure 9 Establishment and Evaluation of AMI Mouse Models. (**A–C**) Histograms of myocardial injury markers CKMB, CTnI, and CK in mice between AMI VS Sham groups; (**D–F**) Histograms of inflammatory markers IL-6, IL-1β, and TNF-α in mice between AMI VS Sham groups; (**G**) TTC staining of the hearts of mice between AMI VS Sham groups; (**H**) HE staining of the hearts of mice between AMI VS Sham groups (Scale bar: 100 μm); (**I**) Immunofluorescence staining of M1 macrophages (CD68, iNOS) as well as M2 macrophages (CD68, CD206) in the myocardium of mice between AMI VS Sham groups (green: iNOS, red: CD68, Orange: CD206; blue: DAPI). (Scale bar: 100 μm), (AMI VS Sham:**p < 0.01; ***p < 0.001).

and IL-4 +shRNA groups (P > 0.05) (Figure 11A). Immunofluorescence analysis showed that the intensity of CD206 fluorescence, which is a marker for M2 signature was highest in the IL-4+shRNA-Ccl9 group, followed by the IL-4 group and IL-4+shRNA. The control group had the lowest intensity, suggesting that knocking down Ccl9 could promote M2 macrophage polarization (Figure 11C). Following RAW264.7-mouse primary cardiomyocyte co-culture, CCK-8 experiments showed that cell viability was significantly higher in the OGD+CM1 group relative to the Control group (P<0.001). There was no significant difference in cell viability between the OGD+CM2 and OGD+CM1 groups

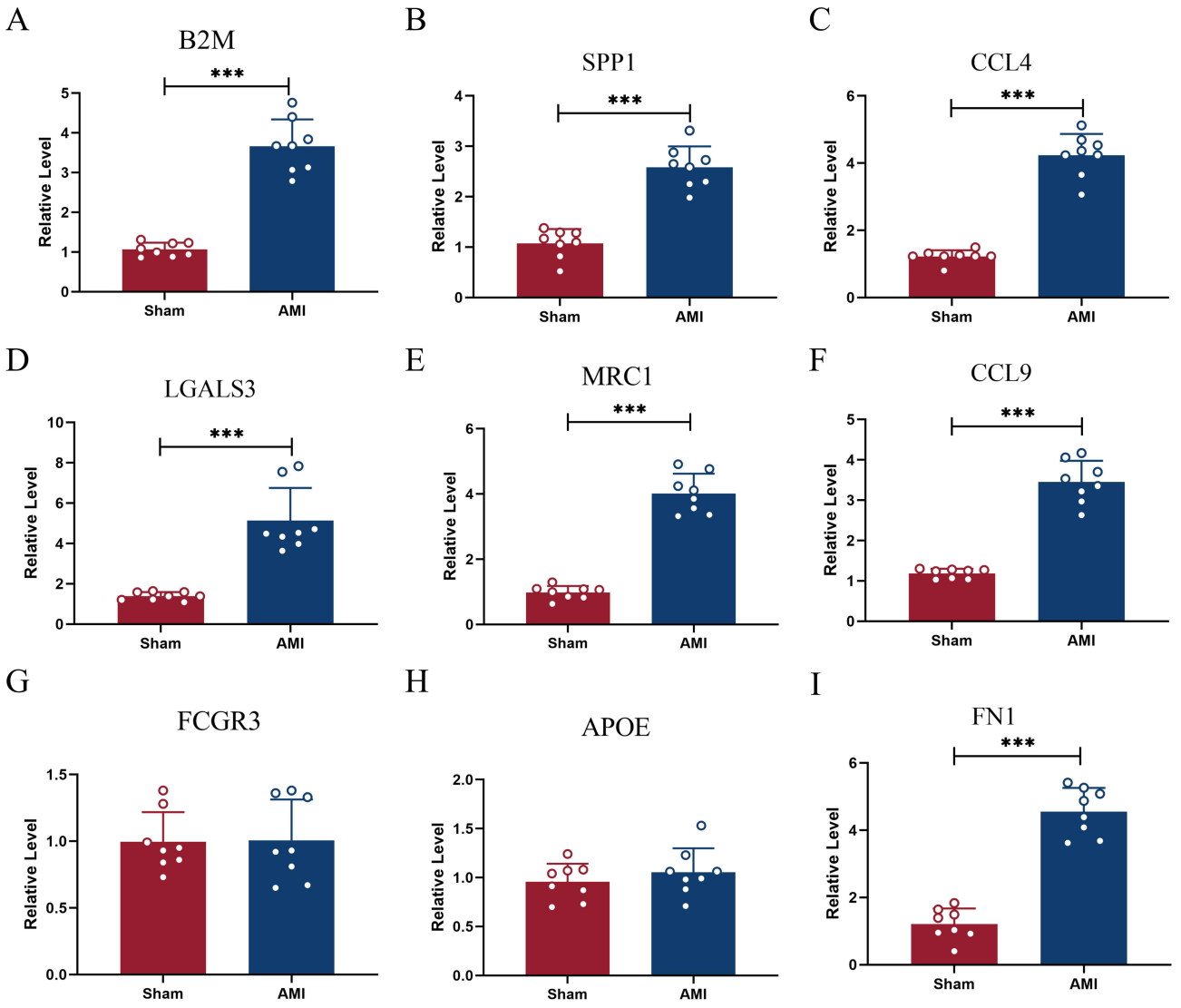

Figure 10 qRT-PCR validation of Monocytes-related hub genes. (**A–I**) Bar graphs of qRT-PCR validation for B2m, Spp1, Ccl4, Lgals3, Mrc1, Ccl9, Fcgr3, Apoe, and Fn1, respectively. (AMI VS Sham: ***p < 0.001).

(P>0.05). However, the OGD+CM3 group exhibited significantly higher cell viability compared to the OGD+CM1 group (P < 0.05) (Figure 11B). Flow cytometry revealed significantly lower apoptosis levels in the OGD+CM1, OGD+CM2, and OGD+CM3 groups relative to the Control group, with the OGD+CM3 group having the lowest apoptosis level (Figure 11D). The aforementioned findings suggest that knockdown of Ccl9 may ameliorate OGD-induced cardiomyocyte injury by promoting macrophage M2 polarization.

Discussion

Myocardial Infarction (AMI) is a disease characterized by acute and persistent myocardial ischemia and consequent myocardial necrosis due to coronary occlusion. It is a major contributor to cardiac fatalities worldwide.[15] Inflammation has been shown to play a major role in the pathophysiological process of AMI, but its pathophysiological mechanisms have not been fully elucidated.[16]

In this study, we explored the potential mechanisms of action and key genes of AMI in regard to inflammation through single cells combined with Bulk transcriptome. The single-cell dataset revealed a total of 18 cell clusters, which were classified into 6 immune cell types: B cells, macrophages, monocytes, neutrophils, NK cells, and T cells. Further differential gene analyses of cellular subpopulations revealed that neutrophils and monocytes exhibited the highest

https://doi.org/10.2147/JIR.S516092

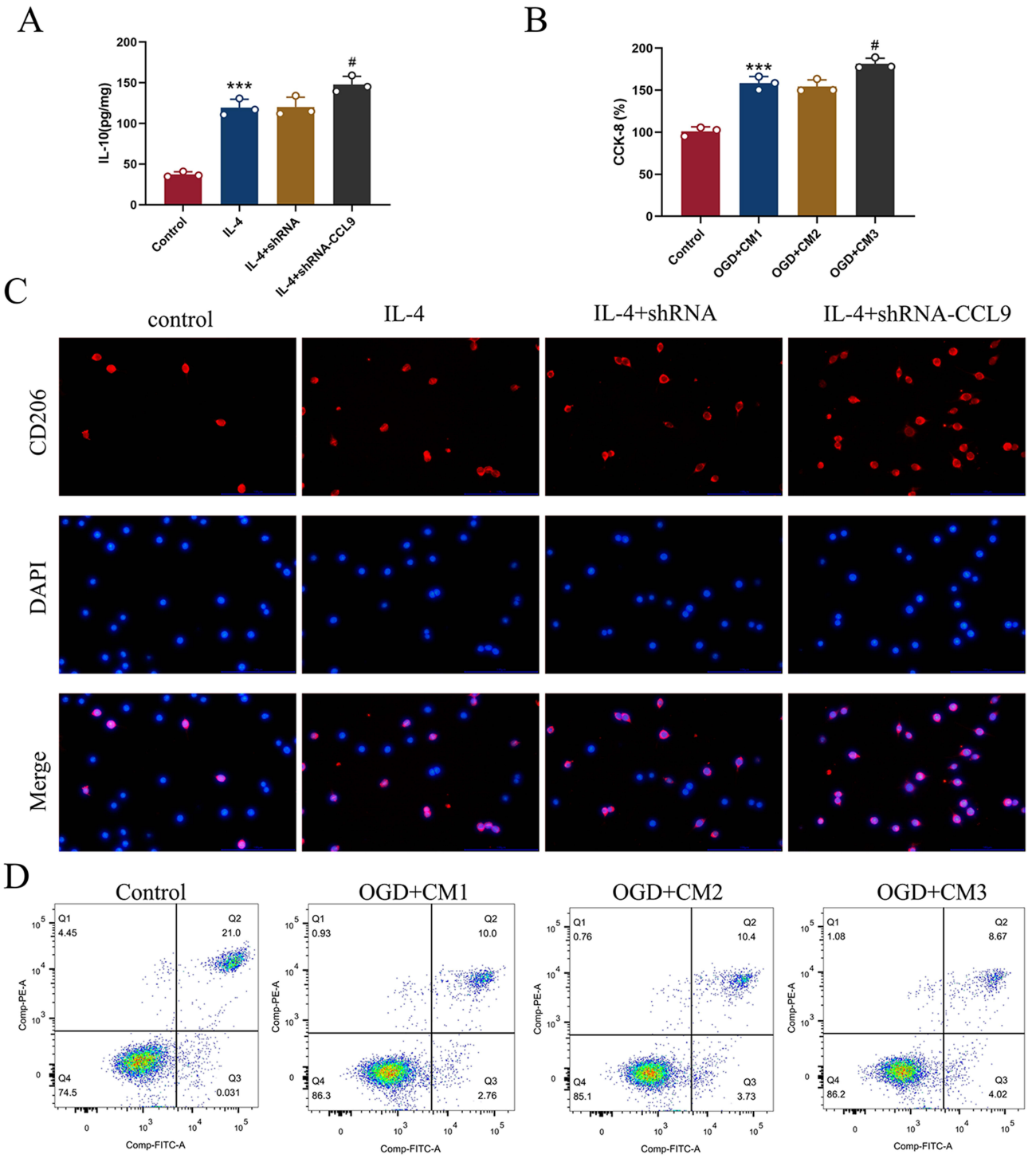

Figure 11 Effect of Ccl9 on the level of sufficient Raw264.7 M2 polarisation and OGD-induced injury in primary mouse cardiomyocytes. (**A**) Histogram of the level of anti-inflammatory factor IL-10 between groups (compared with Control group ***p < 0.001; compared with IL-4 group #p < 0.05); (**B**) Histogram of cell viability between groups (compared with Control group ***p < 0.001; compared with OGD+CM1 group #p < 0.05); (**C**) Immunofluorescence of M2 macrophage marker CD206 immunofluorescence (red: CD206, blue: DAPI); (**D**) Flow Cytometry of apoptosis levels between groups.

amount of differentiated genes when compared to the normal myocardium. The GO enrichment analyses focused on regulation of macrophage migration, regulation of granulocyte chemotaxis, and monocyte differentiation. Intercellular communication analysis revealed that neutrophils and monocytes were active and play a major role in AMI. Therefore

the damage to cardiac tissue in the early stages of AMI generates an acute inflammatory response that initiates the cardiac repair process.[17]

During acute inflammation, a large number of neutrophils activated by pro-inflammatory signals rapidly accumulate in the infarcted area, producing a variety of inflammatory mediators, such as cytokines and chemokines. These neutrophils produce various deleterious products, such as reactive oxygen species and protein hydrolyzing enzymes, which exacerbate the damage to cardiomyocytes and vascular endothelial cells.[18] AMI has the ability to activate the adrenergic pathway and down-regulate hematopoietic stem cell inhibitory factors, which greatly facilitates bone marrow production of monocytes,[19] as a result, circulating monocytes doubled 30 minutes after ischemic injury. Once in the bloodstream monocytes are recruited to the infarct region, where they differentiate and mature into macrophages that release various pro-inflammatory factors.[20] Simultaneously, macrophages transformed from monocytes engage in phagocytosis to eliminate injured cardiomyocytes and promote clearance of neutrophils undergoing apoptosis.[21]

Several studies have documented that a decrease in macrophages in the early stages of inflammation leads to an increase in necrotic cell debris and neutrophils, whereas a decrease in macrophages in the later healing stages prevents collagen deposition and granulation tissue formation.[22] Macrophage depletion leads to increased cardiac fibrosis, hinders neovascularization and inhibits cardiomyocyte proliferation,[22] which is due to the predominance of pro-inflammatory AM1 macrophages in the early stages of inflammation, which is also consistent with the animal findings of the present study. In our study, we found that 3 days after AMI, macrophage infiltration was evident in myocardial tissues of mice, especially M1 macrophages, whereas the late stage of inflammation was mainly dominated by inflammation-suppressing and pro-repairing type M2 macrophages. It has been found that HIMF deficiency promotes macrophage M2 polarization thereby ameliorating acute myocardial ischemic injury.[23] Additionally, it has been found that TRIM21 has the capability to promote macrophage M1 polarization leading to exacerbation of cardiac injury in AMI.[24] Therefore, inhibiting M1 macrophage polarization or promoting M2 macrophage polarization during the acute inflammatory phase of AMI could potentially serve as a novel therapeutic approach for AMI. M1 macrophages dominate early AMI inflammation, exacerbating tissue damage via TNF-α and IL-6 release, while M2 macrophages promote repair through IL-10 and TGF-β.[6,22] Our finding that Ccl9 knockdown enhances M2 polarization (Fig. 12C) aligns with strategies to shift this balance toward repair.

In our study, to screen the key genes related to monocytes, we took the intersection of DEGs of monocytes in the single-cell dataset as well as those in the bulk dataset, which were validated by PPI, correlation analysis, and qRT-PCR. As a result, we identified a total of seven hub genes that are highly relevant to monocytes namely, B2M, SPP1, Ccl4, LGALS3, MRC1, Ccl9, and FN1.

Chemokines are 8–14 kDa proteins that bind to G protein-coupled receptors and exert immunomodulatory effects.[25] Chemokines not only play a key role in the transport of leukocytes to the site of injury, but also mediate gene expression, synthesis of adhesion molecules and changes in cellular conformation.[25] By disrupting the C-C chemokine receptor (CCR)2 signaling, it is possible to inhibit the recruitment of cardiac monocytes in a mouse model of myocarditis, thereby attenuating the inflammatory response in the heart.[26] Previous reports have demonstrated that C-C chemokine ligand (Ccl)17 affects CD4 effector cell and regulatory T cell (Treg) recruitment through activation of the G-protein-coupled receptor CCR4.[27] Ccl signaling has been implicated in a number of inflammatory diseases such as asthma, dermatitis, colitis, arthritis, and atherosclerosis.[27] In addition, it has been found that C-C chemokine ligands are strongly associated with macrophage polarization. Various studies have discovered that elevated levels of Ccl2, M1-type tumor-associated macrophages polarized towards M2 type.[28] It has also been found that knockdown of Ccl7 in lung adenocarcinoma inhibited the level of M2 polarization of macrophages.[29] Thus, the chemokine family has the ability to impact the degree of macrophage polarization and regulating leukocyte transport, which may be a promising therapeutic target to modulate the inflammatory response, thus avoiding the damage caused by excessive inflammatory response.

Currently, numerous researchers have observed that myocardial tissues after AMI are accompanied by significant up-regulation of chemokine expression, however the mechanism of action remains unclear.[30–32] Ccl9 is an important chemokine that plays a major role in anti-tumor metastasis and inhibition of tumor growth.[33,34] Nevertheless, the mechanism of action of Ccl9 in AMI is unclear. Therefore, Ccl9 was selected for subsequent cellular experiments to investigate the potential mechanism of action in AMI in our study. It is well known that after the occurrence of AMI, the

necrotic myocardium induces an intense inflammatory response, which recruits peripherally circulating monocytes to myocardial tissues, which are rapidly transformed into macrophages to play their roles in removing necrotic cell debris from the infarcted area of the myocardium, thus promoting wound healing and scar formation. They are considered to be one of the most important inflammatory cells.[35] Therefore, macrophages (Raw264.7) were selected for cellular experiments in this study.[36,37]

Our study findings demonstrated that low expression of Ccl9 promoted the polarization of M2 macrophages by interfering with the expression level of Ccl9 in Raw264.7 cells during M2 macrophage induction. Subsequently, we established an OGD model using mouse primary cardiomyocytes and cultured them with conditioned culture medium and found that Ccl9 may affect OGD-induced cardiomyocyte injury by modulating the level of macrophage M2 polarization. Consistent with our findings, several studies have shown that M2 macrophages are beneficial for cardiac tissue repair.[38,39] Hence, it is crucial to develop treatment approaches that enhance the polarization of macrophages towards the M2 phenotype in AMI.

Undoubtedly, this study is subject to numerous limitations. Firstly, this study was conducted only at the animal cell level and was not validated in more depth at the clinical level. Furthermore, this study did not tap into the specific pathways of interaction between monocytes/macrophages and cardiomyocytes. Additionally, this study has not yet fully explored the interactions between CCL9 and the other eight genes. This will be a key focus for future research. Therefore, the specific mechanisms associated with monocytes/macrophages in AMI still need to be further investigated.

Conclusion

Our study revealed the relevant genes in monocytes/macrophages in AMI: B2M, SPP1, Ccl4, LGALS3, MRC1, Ccl9, and FN1 by using single cells combined with Bulk transcriptome analysis and validated by animal experiments. Further, Ccl9 was selected to probe the mechanism in this study. A series of cellular experiments were performed, revealing that Ccl9 might has the potential to regulate the macrophage M2 polarization level and affect OGD-induced cardiomyocyte injury. Consequently, Ccl9 is believed to play a role in AMI. Our study enriches the pathophysiological mechanisms associated with AMI inflammation and provides a partial basis for finding new therapeutic avenues for AMI.

Data Sharing Statement

The datasets GSE158157, GSE23294 and GSE163129 used in the current study are available in the GEO repository (https://www.ncbi.nlm.nih.gov/geo/).

Ethical Approval and Consent to Participate

The animal protocol for this study was approved by the Institutional Animal Care and Use Committee (ZJCLA-IACUC -20010502). This study utilized publicly available datasets (GSE158157, GSE23294, GSE163129) from GEO. According to Article 32 of China's "Measures for Ethical Review of Life Science and Medical Research Involving Human Subjects" (2023), research using anonymized public data is exempt from institutional ethics approval.

Acknowledgments

We extended our gratitude to all the participants who contributed to this article.

Author Contributions

All authors made a significant contribution to the work reported, whether that is in the conception, study design, execution, acquisition of data, analysis and interpretation, or in all these areas; took part in drafting, revising or critically reviewing the article; gave final approval of the version to be published; have agreed on the journal to which the article has been submitted; and agree to be accountable for all aspects of the work.

Funding

There is no funding to report.

Disclosure

There is no conflict of interest.

References

1. Blinnikova K, Cohen CW, McKeag ID. Lifestyle intervention for the prevention of cardiovascular disease. *Prim Care*. 2024;51(1):13–26. doi:10.1016/j.pop.2023.07.001
2. Schmitz T, Harmel E, Raake PP, et al. Association between acute myocardial infarction symptoms and short- and long-term mortality after the event. *Can J Cardiol*. 2024;40(7):1355–1366. doi:10.1016/j.cjca.2024.01.019
3. Del Buono MG, Bonaventura A, Vecchié A, et al. Pathogenic pathways and therapeutic targets of inflammation in heart diseases: a focus on Interleukin-1. *Eur J Clin Invest*. 2024;54(2):e14110. doi:10.1111/eci.14110
4. Schelemei P, Wagner E, Picard FSR, et al. Macrophage mediators and mechanisms in cardiovascular disease. *FASEB J*. 2024;38(2):e23424. doi:10.1096/fj.202302001R
5. Zuo W, Sun R, Ji Z, et al. Macrophage-driven cardiac inflammation and healing: insights from homeostasis and myocardial infarction. *Cell Mol Biol Lett*. 2023;28(1):81. doi:10.1186/s11658-023-00491-4
6. Jian Y, Zhou X, Shan W, et al. Crosstalk between macrophages and cardiac cells after myocardial infarction. *Cell Commun Signal*. 2023;21(1):109. doi:10.1186/s12964-023-01105-4
7. Arif M, Klevstig M, Benfeitas R, et al. Integrative transcriptomic analysis of tissue-specific metabolic crosstalk after myocardial infarction. *Elife*. 2021;10. doi:10.7554/eLife.66921
8. Long H, Steimle JD, Grisanti Canozo FJ, et al. Endothelial cells adopt a pro-reparative immune responsive signature during cardiac injury. *Life Sci Alliance*. 2024;7(2):e202201870. doi:10.26508/lsa.202201870
9. Jung SH, Hwang BH, Shin S, et al. Spatiotemporal dynamics of macrophage heterogeneity and a potential function of Trem2(hi) macrophages in infarcted hearts. *Nat Commun*. 2022;13(1):4580. doi:10.1038/s41467-022-32284-2
10. Pradeep SR, Thirunavukkarasu M, Accorsi D, et al. Novel approaches to determine the functional role of cardiomyocyte specific E3 ligase, Pellino-1 following myocardial infarction. *Biochim Biophys Acta Mol Basis Dis*. 2024;1870(1):166899. doi:10.1016/j.bbadis.2023.166899
11. Qin C, Wang T, Qian N, et al. Epigallocatechin gallate prevents cardiomyocytes from pyroptosis through lncRNA MEG3/TAF15/AIM2 axis in myocardial infarction. *Chin Med*. 2023;18(1):160. doi:10.1186/s13020-023-00856-z
12. Nie S, Cui X, Guo J, et al. Long non-coding RNA AK006774 inhibits cardiac ischemia-reperfusion injury via sponging miR-448. *Bioengineered*. 2021;12(1):4972–4982. doi:10.1080/21655979.2021.1954135
13. Chen J, Chen S, Cai D, et al. The role of Sirt6 in osteoarthritis and its effect on macrophage polarization. *Bioengineered*. 2022;13(4):9677–9689. doi:10.1080/21655979.2022.2059610
14. Sun F, Guo Z, Zhang C, et al. LncRNA NRON alleviates atrial fibrosis through suppression of M1 macrophages activated by atrial myocytes. *Biosci Rep*. 2019;39(11). doi:10.1042/BSR20192215
15. Lopez-Lopez JP, Toro MR, Martinez-Bello D, et al. Sex differences in cardiovascular disease risk factor prevalence, morbidity, and mortality in colombia: findings from the Prospective Urban Rural Epidemiology (PURE) Study. *Glob Heart*. 2024;19(1):10. doi:10.5334/gh.1289
16. Madanchi M, Young M, Tersalvi G, et al. The impact of colchicine on patients with acute and chronic coronary artery disease. *Eur J Intern Med*. 2024;125:1–9. doi:10.1016/j.ejim.2024.01.004
17. Zhang H, Dhalla NS. The role of pro-inflammatory cytokines in the pathogenesis of cardiovascular disease. *Int J Mol Sci*. 2024;25(2):1082.
18. Zhang N, Aiyasiding X, Li WJ, et al. Neutrophil degranulation and myocardial infarction. *Cell Commun Signal*. 2022;20(1):50. doi:10.1186/s12964-022-00824-4
19. Oliveira JB, Soares A, Sposito AC. Inflammatory response during myocardial infarction. *Adv Clin Chem*. 2018;84:39–79.
20. Alvarez-Argote S, O'Meara CC. The evolving roles of cardiac macrophages in homeostasis, regeneration, and repair. *Int J Mol Sci*. 2021;22(15):7923. doi:10.3390/ijms22157923
21. Nian W, Huang Z, Fu C. Immune cells drive new immunomodulatory therapies for myocardial infarction: from basic to clinical translation. *Front Immunol*. 2023;14(1097295). doi:10.3389/fimmu.2023.1097295
22. Shook PL, Singh M, Singh K. Macrophages in the inflammatory phase following myocardial infarction: role of exogenous ubiquitin. *Biology*. 2023;12(9):1258. doi:10.3390/biology12091258
23. Li Y, Dong M, Wang Q, et al. HIMF deletion ameliorates acute myocardial ischemic injury by promoting macrophage transformation to reparative subtype. *Basic Res Cardiol*. 2021;116(1):30. doi:10.1007/s00395-021-00867-7
24. Li Z, Liu X, Zhang X, et al. TRIM21 aggravates cardiac injury after myocardial infarction by promoting M1 macrophage polarization. *Front Immunol*. 2022;13:1053171.
25. Matsushima K, Yang D, Oppenheim JJ. Interleukin-8: an evolving chemokine. *Cytokine*. 2022;153(155828):155828. doi:10.1016/j.cyto.2022.155828
26. Hanna A, Frangogiannis NG. Inflammatory cytokines and chemokines as therapeutic targets in heart failure. *Cardiovasc Drugs Ther*. 2020;34(6):849–863. doi:10.1007/s10557-020-07071-0
27. Feng G, Zhu C, Lin CY, et al. CCL17 protects against viral myocarditis by suppressing the recruitment of regulatory T cells. *J Am Heart Assoc*. 2023;12(4):e028442. doi:10.1161/JAHA.122.028442
28. Chiang Y, Tsai YC, Wang CC, et al. Tumor-derived C-C motif ligand 2 induces the recruitment and polarization of tumor-associated macrophages and increases the metastatic potential of bladder cancer cells in the postirradiated microenvironment. *Int J Radiat Oncol Biol Phys*. 2022;114(2):321–333. doi:10.1016/j.ijrobp.2022.06.054
29. Wu Z, Bai X, Lu Z, et al. LINC01094/SPI1/CCL7 axis promotes macrophage accumulation in lung adenocarcinoma and tumor cell dissemination. *J Immunol Res*. 2022;2022(6450721):1–19. doi:10.1155/2022/6450721
30. Shen SC, Xu J, Cheng C, et al. Macrophages promote the transition from myocardial ischemia reperfusion injury to cardiac fibrosis in mice through GMCSF/CCL2/CCR2 and phenotype switching. *Acta Pharmacol Sin*. 2024;45:959–74. doi:10.1038/s41401-023-01222-3

31. Wang W, Chen XK, Zhou L, et al. Chemokine CCL2 promotes cardiac regeneration and repair in myocardial infarction mice via activation of the JNK/STAT3 axis. *Acta Pharmacol Sin*. 2023. doi:10.1038/s41401-023-01198-0
32. Zhang J, Hao W, Zhang J, et al. CXCL16 promotes Ly6Chigh monocyte infiltration and impairs heart function after acute myocardial infarction. *J Immunol*. 2023;210(6):820–831. doi:10.4049/jimmunol.2200249
33. Łazarczyk M, Kurzejamska E, Mickael ME, et al. Mouse CCL9 chemokine acts as tumor suppressor in a murine model of colon cancer. *Curr Issues Mol Biol*. 2023;45(4):3446–3461. doi:10.3390/cimb45040226
34. Yan HH, Jiang J, Pang Y, et al. CCL9 induced by TGFβ signaling in myeloid cells enhances tumor cell survival in the premetastatic organ. *Cancer Res*. 2015;75(24):5283–5298. doi:10.1158/0008-5472.CAN-15-2282-T
35. Nayak TK, Bajpai A, Patwa V, et al. Loss of myeloid cell-specific β2-adrenergic receptor expression ameliorates cardiac function and remodeling after acute ischemia. *bioRxiv*. 2023. doi:10.1101/2023.11.27.568873
36. Niu XH, Liu RH, Lv X, et al. Activating α7nAChR helps post-myocardial infarction healing by regulating macrophage polarization via the STAT3 signaling pathway. *Inflamm Res*. 2023;72(4):879–892. doi:10.1007/s00011-023-01714-2
37. Tang C, Wang L, Sheng Y, et al. CLEC-2-dependent platelet subendothelial accumulation by flow disturbance contributes to atherogenesis in mice. *Theranostics*. 2021;11(20):9791–9804. doi:10.7150/thno.64601
38. Chen L, Pan D, Zhang Y, et al. C-C motif chemokine 2 regulates macrophage polarization and contributes to myocardial infarction healing. *J Interferon Cytokine Res*. 2023;44(2):68–79. doi:10.1089/jir.2023.0132
39. Guo M, Xia Z, Hong Y, et al. The TFPI2-PPARγ axis induces M2 polarization and inhibits fibroblast activation to promote recovery from post-myocardial infarction in diabetic mice. *J Inflamm*. 2023;20(1):35. doi:10.1186/s12950-023-00357-8